Pharmacological silencing of nasal TRPV1⁺ nociceptors ameliorates eosinophilic infiltration but exacerbates neutrophilic infiltration in murine models of allergic rhinitis

Fan Ye*,[1,3,5], Ying Tao*,[2], Junhai Chen*, [1,3,5], Ruizhi Wang[1,3,5], Yiwen Li[1,3,5], Zhaohui Shi[1,3,4,5], Qintai Yang[1,3,4,5]

Rhinology 64: 5, 0 - 0, 2026
https://doi.org/10.4193/Rhin25.667

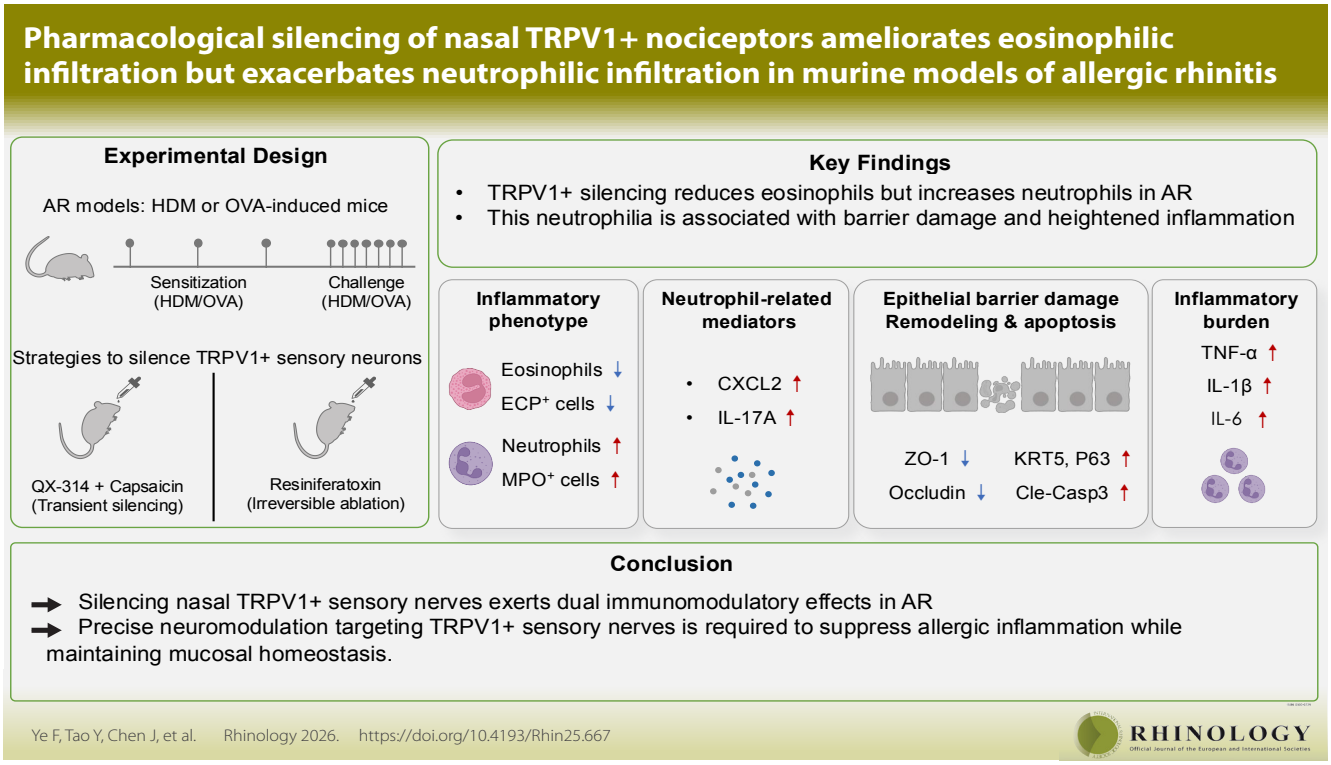

Abstract

Background: The pathogenesis of allergic rhinitis (AR) involves hyperreactivity of both the immune and neural systems. While sensory nerves detect allergens and release neuropeptides that directly participate in immune regulation, their precise role within the AR inflammatory network remains incompletely elucidated. **Methodology**: Using house dust mite (HDM) and ovalbumin (OVA)-induced murine AR models, we selectively silenced nasal TRPV1-expressing sensory nerves pharmacologically with QX-314 (co-administered with capsaicin) and Resiniferatoxin (RTX). The effects of neuronal silencing on animal behavior, allergen-specific IgE levels, inflammatory cell infiltration, and immune cell populations were systematically evaluated via immunofluorescence, histological staining, ELISA, and flow cytometry. **Results**: Both QX-314 and RTX effectively silenced TRPV1⁺ sensory neurons in the trigeminal ganglia and significantly downregulated the expression of neuropeptides CGRP and SP. Silencing nasal TRPV1⁺ sensory nerves markedly reduced eosinophilic infiltration and levels of the associated marker ECP in the nasal mucosa of AR model mice. Unexpectedly, it also led to a significant increase in neutrophilic infiltration and MPO-positive cells. RTX-mediated ablation further compromised epithelial barrier integrity and aggravated the local inflammatory burden. Flow cytometric analysis further confirmed that RTX-mediated ablation of TRPV1⁺ neurons significantly decreased the proportions of infiltrating eosinophils and B cells, but increased the proportion of neutrophils in the OVA model. **Conclusions**: Silencing nasal TRPV1⁺ sensory nerves exerts a dual immunomodulatory effect in AR, attenuating eosinophilic inflammation while promoting neutrophilic infiltration. This reveals a critical neuro-immune balance in the nasal mucosa and suggests that precisely targeted neuromodulation strategies are required to suppress allergic inflammation.

Key words: allergic rhinitis, neuroimmunology, nociceptors, eosinophils, neutrophils

Corrected Proof

Introduction

Allergic rhinitis is recognized as a disorder characterized by both immune dysregulation and neural hyperreactivity [1,2]. Hypersensitivity of sensory and parasympathetic nerves innervating the nasal mucosa gives rise to hallmark symptoms of allergic rhinitis, such as nasal itching, sneezing, and rhinorrhea [3,4]. Notably, sensory nerves not only detect environmental irritants, allergens, and cytokines, but also release neuropeptides that directly participate in immune regulation, potentially playing a pivotal role in the pathogenesis of this condition [1,5]. Upregulation of sensory nerve markers and neuropeptides has been observed in the nasal mucosa of allergic rhinitis patients and is associated with more severe clinical symptoms [4,6,7].

Nociceptors, a specialized subset of sensory neurons, express transient receptor potential vanilloid 1 (TRPV1)—a non-selective cation channel activated by diverse stimuli including heat, capsaicin, and inflammatory mediators [8,9]. Upon activation, nociceptor terminals release neuropeptides such as calcitonin gene-related peptide (CGRP, encoded by Calca) and substance P (SP, encoded by Tac1), which can either amplify or suppress downstream inflammatory cascades [9-12]. Despite recent advances in understanding neuro-immune crosstalk, whether nociceptors regulate the development, severity, and/or resolution of allergic rhinitis remains to be fully elucidated.

In this study, we established house dust mite (HDM) and ovalbumin (OVA)-induced murine models of allergic rhinitis and pharmacologically silenced TRPV1-expressing sensory nerves in the nasal cavity using QX-314 and Resiniferatoxin (RTX). Our results demonstrate that silencing nasal TRPV1$^+$ sensory nerves reduced eosinophil infiltration but increased neutrophil infiltration in the nasal mucosa of AR model mice. These findings underscore a critical role for sensory nerves in modulating nasal mucosal inflammation.

Materials and methods

For detailed methods, see Supplementary Material

Animals and allergic rhinitis models

BALB/c mice were purchased from the Guangdong Provincial Experimental Animal Center and housed in a specific pathogen-free facility. All protocols were approved by the IACUC of Sun Yat-Sen University (Approval No. SYSU-IACUC-2025-B2045). To establish HDM- or OVA-induced AR models, mice were sensitized via i.p. injection of 200 µL saline containing 100 µg HDM or 50 µg OVA adsorbed to 2 mg aluminum hydroxide on days 0, 7, and 14. From days 21 to 27, nasal inflammation was elicited by intranasal administration of 10 µL (5 µL/nostril) saline containing 50 µg HDM or 1 mg OVA without anesthesia [13,14]. Control mice received saline. After the final challenge, videos were recorded and analyzed by a blinded investigator to count sneezes and nasal rubbings.

Silencing of nasal sensory nerves with QX-314 or resiniferatoxin (RTX)

QX-314, a positively charged lidocaine derivative, acts as a sodium channel blocker that inhibits the activity of Nav1.8-expressing nociceptive neurons [15,16]. Its entry into neurons is dependent on the opening of TRP channels [15,16]. To inhibit TRPV1-expressing sensory nerves, a mixture of 10 µL capsaicin (a TRPV1 receptor agonist;) and 1% QX-314 was administered intranasally [16-18]. This mixture was given 1 hour before each nasal allergen challenge. The control group received an equal volume of 0.9% saline containing 1% (v/v) DMSO. RTX, a potent TRPV1 agonist, induces irreversible neuronal depolarization [19]. Mice received intranasal RTX in an escalating dose regimen (30, 70, and 100 µg/kg) over three consecutive days [19,20], followed by a 14-day rest period before subsequent experiments. Control mice for this experiment were treated with an equal volume of 0.9% saline containing 1% (v/v) DMSO.

Statistical analysis

Statistical analyses were performed using Prism version 9 (GraphPad Software). Data are presented as mean and 95% CI. Two-sided Student's t-tests (with FDR correction for time-course comparisons) were used for two-group comparisons, and one-way ANOVA for multiple groups. $P < 0.05$ was considered significant.

Results

QX-314–induced sensory silencing increases neutrophilic infiltration in the nasal mucosa of AR mice

To assess the role of TRPV1-expressing sensory neurons in AR, we utilized QX-314 co-administered with capsaicin, a TRPV1 agonist [16]. The results showed that after seven consecutive days of QX-314 treatment, the expression levels of TRPV1 and Nav1.8 were not significantly altered (Figures 1A, 1C, and 1D). However, there was a significant reduction in the number of neurons positive for the neuropeptides CGRP and SP compared to the control group (Figures 1B, 1E, and 1F), indicating that QX-314 effectively suppressed sensory neuron activation.

Subsequently, we established OVA- and HDM-induced AR mouse models as described in the Methods section. A mixture of QX-314 and capsaicin was administered intranasally 1 hour before each allergen challenge; the control group received vehicle (Figure 1G). QX-314 significantly alleviated allergen-induced sneezing and nasal rubbing compared to the control (Figures 1H and 1I), but did not affect serum levels of allergen-specific IgE (Figure 1J) (21). H&E staining showed that QX-314 did not alter baseline eosinophil numbers; in both HDM- and OVA-induced models, QX-314 led to a slight reduction in eosinophil numbers (Figures 2A and 2B). The number of goblet cells and mucin content per goblet cell were unchanged (Figures 2C-2E).

Corrected Proof

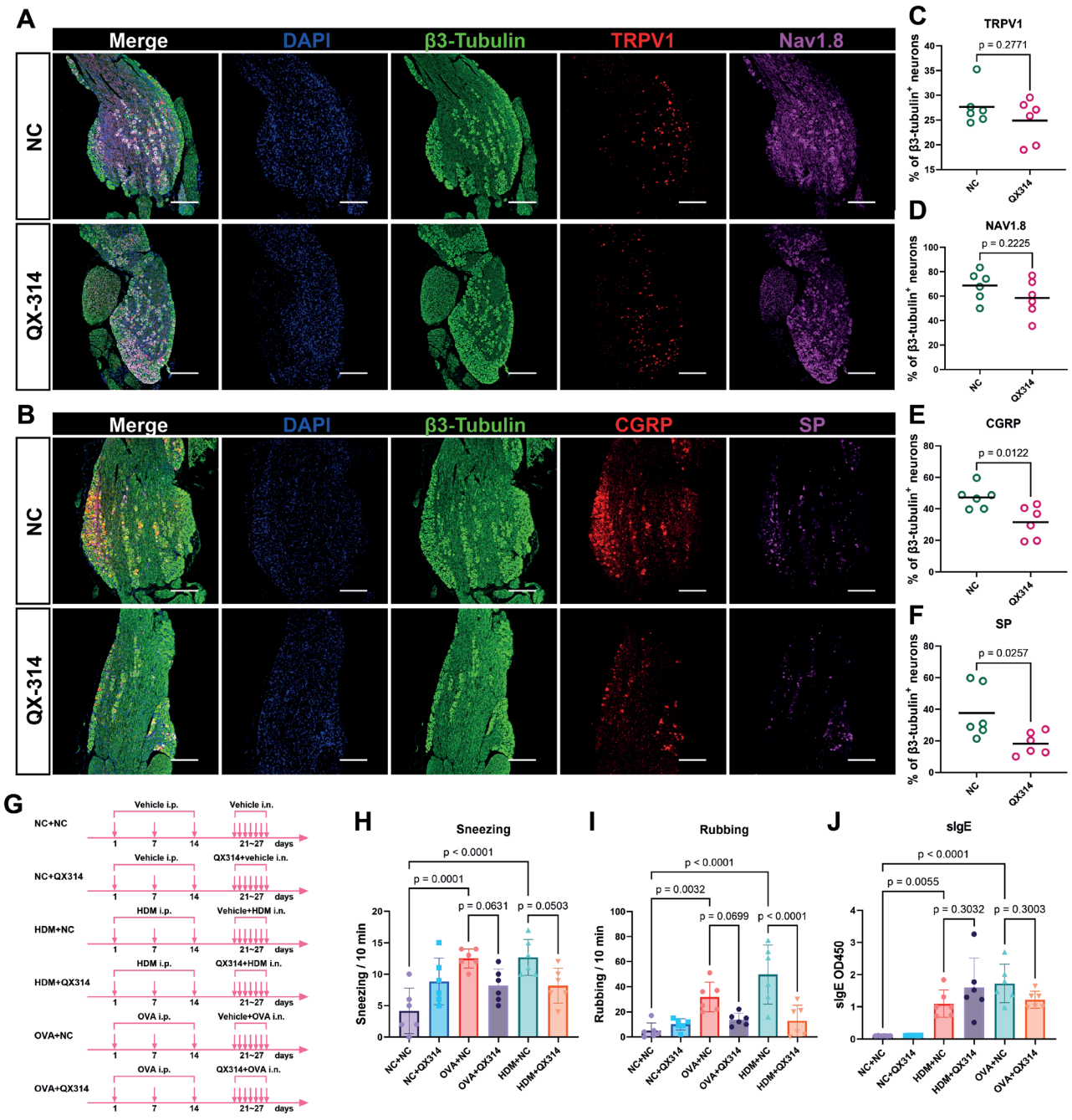

Figure 1. QX-314–induced silencing of trigeminal TRPV1⁺ sensory nerves. (A-B) Immunofluorescence staining for TRPV1, Nav1.8, CGRP, and SP in trigeminal ganglion neurons following 7-day intranasal co-treatment with QX-314 and capsaicin. Scale bar = 250 μm. (C-F) Quantification of the proportion of neurons positive for TRPV1, Nav1.8, CGRP, and SP. (G) Schematic of the AR model and treatment timeline. Mice were sensitized via three intraperitoneal (i.p.) injections of HDM or OVA adsorbed to 2 mg aluminum hydroxide at weekly intervals, followed by seven consecutive days of intranasal challenge with HDM or OVA. Control mice received vehicle. QX-314 (co-administered with capsaicin) or vehicle control was administered intranasally 1 hour before each challenge. (H-I) The number of sneezes and nasal rubbing episodes was recorded for 10 minutes after the final challenge. (J) Serum levels of HDM- or OVA-specific IgE (sIgE) were measured by ELISA. Data for groups "NC+NC", "NC+QX314", "HDM+NC", and "HDM+QX314" show HDM-sIgE levels; data for groups "OVA+NC" and "OVA+QX314" show OVA-sIgE levels. Ordinary one-way ANOVA was used for comparisons among multiple groups, and two-sided Student's t-tests were used for comparisons between two groups. Data are presented as mean and 95% confidence interval. Abbreviations: CGRP, calcitonin gene-related peptide; SP, substance P; TRPV1, transient receptor potential vanilloid 1; Nav1.8, voltage-gated sodium channel 1.8.

Corrected Proof

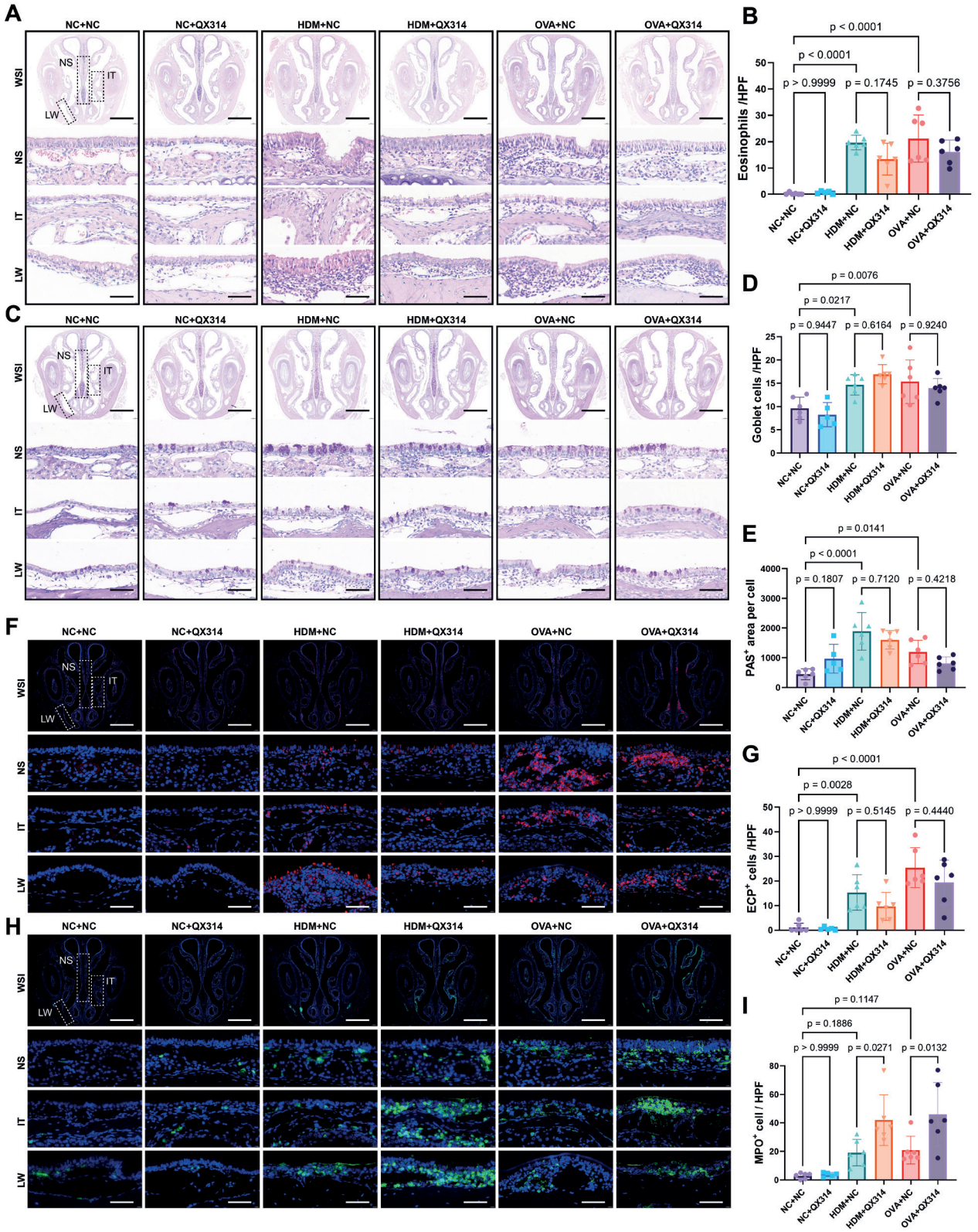

Figure 2. QX-314–induced sensory silencing increases neutrophilic infiltration in the nasal mucosa of AR mice. (A) Representative H&E staining of nasal mucosa and (B) quantitative analysis of eosinophil numbers. (C) PAS staining of nasal mucosa, with quantification of (D) goblet cell numbers and (E) mucin content per goblet cell. (F) Representative immunofluorescence staining for ECP and (G) quantification of ECP-positive cells. (H) Representative immunofluorescence staining for MPO and (I) quantification of MPO-positive cells. Whole-slide images (WSI) and representative images from specific anatomical regions—nasal septum (NS), inferior turbinate (IT), and lateral wall (LW)—are shown. Scale bar: 2 mm for WSI; 50 μm for other images. Ordinary one-way ANOVA was used for comparisons among multiple groups. Data are presented as mean and 95% confidence interval. Abbreviations: ECP, eosinophil cationic protein; MPO, myeloperoxidase; PAS, periodic acid-Schiff.

Corrected Proof

Eosinophil cationic protein (ECP) is primarily expressed in eosinophils [22,23], and Myeloperoxidase (MPO) is primarily expressed in neutrophils [24]. To further investigate changes in eosinophil and neutrophil numbers, we performed ECP and MPO staining on tissue sections. The results indicated that under baseline conditions, QX-314 treatment did not increase the numbers of ECP-positive or MPO-positive cells in the nasal mucosa (Figures 2F-2I). However, in HDM- or OVA-induced models, pretreatment with intranasal QX-314 resulted in a slight decrease in ECP-positive cells but a significant increase in MPO-positive cells compared to the saline control (Figures 2F-2I). Together, blockade of sensory nerves with QX-314 promoted a shift in AR inflammation towards neutrophilic infiltration.

Silencing of TRPV1$^+$ sensory neurons by RTX reduces eosinophilic but enhances neutrophilic infiltration in the nasal mucosa of AR mice

To further confirm the immunomodulatory role of silencing TRPV1$^+$ sensory nerves in AR, we used RTX, an irreversible and potent TRPV1 agonist [19]. Mice received intranasal RTX in an escalating dose regimen over three consecutive days (see Methods). Trigeminal ganglia were collected 6 weeks after the completion of RTX treatment. Immunostaining revealed that, compared to the control group, RTX treatment significantly reduced the number of TRPV1$^+$ neurons in the trigeminal ganglia, accompanied by a marked decrease in SP- and CGRP-expressing neurons, while Nav1.8 expression remained unchanged (Figures 3A-3F). These results suggest that RTX treatment stably and irreversibly ablates TRPV1$^+$ neurons.

We next investigated the impact of RTX-induced sensory nerve ablation on AR inflammation. Mice were allowed to rest for 2 weeks after RTX treatment before establishing HDM- and OVA-induced AR models (Figure 3G). Interestingly, unlike QX-314, RTX treatment did not alleviate allergen challenge-induced sneezing or nasal scratching compared to the control group (Figures 3H and 3I). Consistent with the QX-314 findings, RTX treatment had no significant effect on serum levels of specific IgE (Figure 3J).

To investigate the differential effects of RTX and QX-314 on AR symptoms, we immunostained trigeminal ganglia for TRPA1, SST, and HRH1 (Figure S1A)—sensory neuron markers associated with nose rubbing, sneezing, and itching [4,25-28]. Notably, although RTX significantly reduced the number of TRPV1-positive neurons (Figure 3C), it led to a marked increase in the proportion of TRPA1-positive neurons compared with the control condition (Figure S1B). HRH1 expression remained unchanged after RTX treatment (Figure S1C). Similar to TRPV1, SST-positive neurons were substantially decreased following RTX treatment (Figure S1D). In contrast, QX314 treatment did not significantly alter the proportion of any of the above neuronal subtypes (Figures S1B-S1D). To further assess neuronal activation, we measured p-ERK1/2 expression [9]. Multiplex immunofluorescence (see Methods for details; a representative image is shown in Figures S2A and S2B) showed that RTX reduced the proportion of activated (p-ERK1/2$^+$) TRPV1$^+$ and SST$^+$ neurons but increased activated TRPA1$^+$ and HRH1$^+$ neurons (Figures S1E–S1H). In contrast, QX-314 reduced activated TRPV1$^+$, TRPA1$^+$, and HRH1$^+$ neurons (Figures S1E–S1H). Thus, RTX-mediated TRPV1 ablation leads to compensatory activation of TRPA1$^+$ and HRH1$^+$ neurons, whereas QX-314 suppresses activation across all three subsets without altering their abundance.

Next, we analyzed the pathological features of AR following RTX treatment. Under baseline conditions, RTX treatment did not alter eosinophil numbers in the nasal mucosa compared to control (Figures 4A and 4B). However, in both HDM- and OVA-induced models, RTX treatment significantly reduced nasal eosinophil infiltration compared to the control (Figures 4A and 4B). In line with the QX-314 results, RTX did not affect the number of goblet cells or the mucin content per goblet cell (Figures 4C-4E). Immunofluorescence staining demonstrated that in HDM- or OVA-induced models, RTX treatment significantly decreased the infiltration of ECP$^+$ cells while significantly increasing the number of MPO$^+$ cells compared to the control (Figures 4F-4I).

Finally, since our histological analysis revealed more pronounced changes in the OVA-induced model, we selected the RTX-treated OVA model for validation by flow cytometry. A multiparameter flow cytometry panel was used to distinguish T cells (CD45$^+$CD3$^+$), CD4$^+$ T cells (CD45$^+$CD3$^+$CD4$^+$), CD8$^+$ T cells (CD45$^+$CD3$^+$CD8$^+$), B cells (CD45$^+$CD19$^+$), eosinophils (CD45$^+$CD11b$^+$Siglec-F$^+$) [29], and neutrophils (CD45$^+$CD11b$^+$Ly6G$^+$) [30] in the nasal mucosa (Figure 5A). The results showed that, compared to the control, RTX treatment significantly reduced eosinophil infiltration but markedly increased the proportion of neutrophils in the nasal mucosa of OVA-model mice (Figures 5B and 5C). The infiltration of CD19$^+$B cells and CD4$^+$T cells was also reduced in the RTX-treated group (Figures 5D and 5F). No significant differences were observed in total T cell or CD8$^+$T cell numbers between the RTX-treated and control groups (Figures 5E and 5G). To investigate the dynamic changes of eosinophils and neutrophils in the nasal mucosa of the OVA-induced AR model following RTX treatment, we performed flow cytometry analysis on days 1, 3, 5, and 7 of continuous allergen challenge (Figure 5H). The results showed that a significant difference in eosinophil counts between the RTX and control groups was first detected on day 5 (Figure 5I). In contrast, a marked increase in neutrophils in the RTX-treated group was observed as early as day 3 (Figure 5J). These findings indicate that in RTX-induced nasal mucosal immune remodeling, changes in neutrophil abundance precede those of eosinophils.

In summary, our results demonstrate that silencing TRPV1-expressing sensory nerves alleviates eosinophilic infiltration but conversely promotes neutrophilic inflammation in the nasal mucosa of AR models.

Corrected Proof

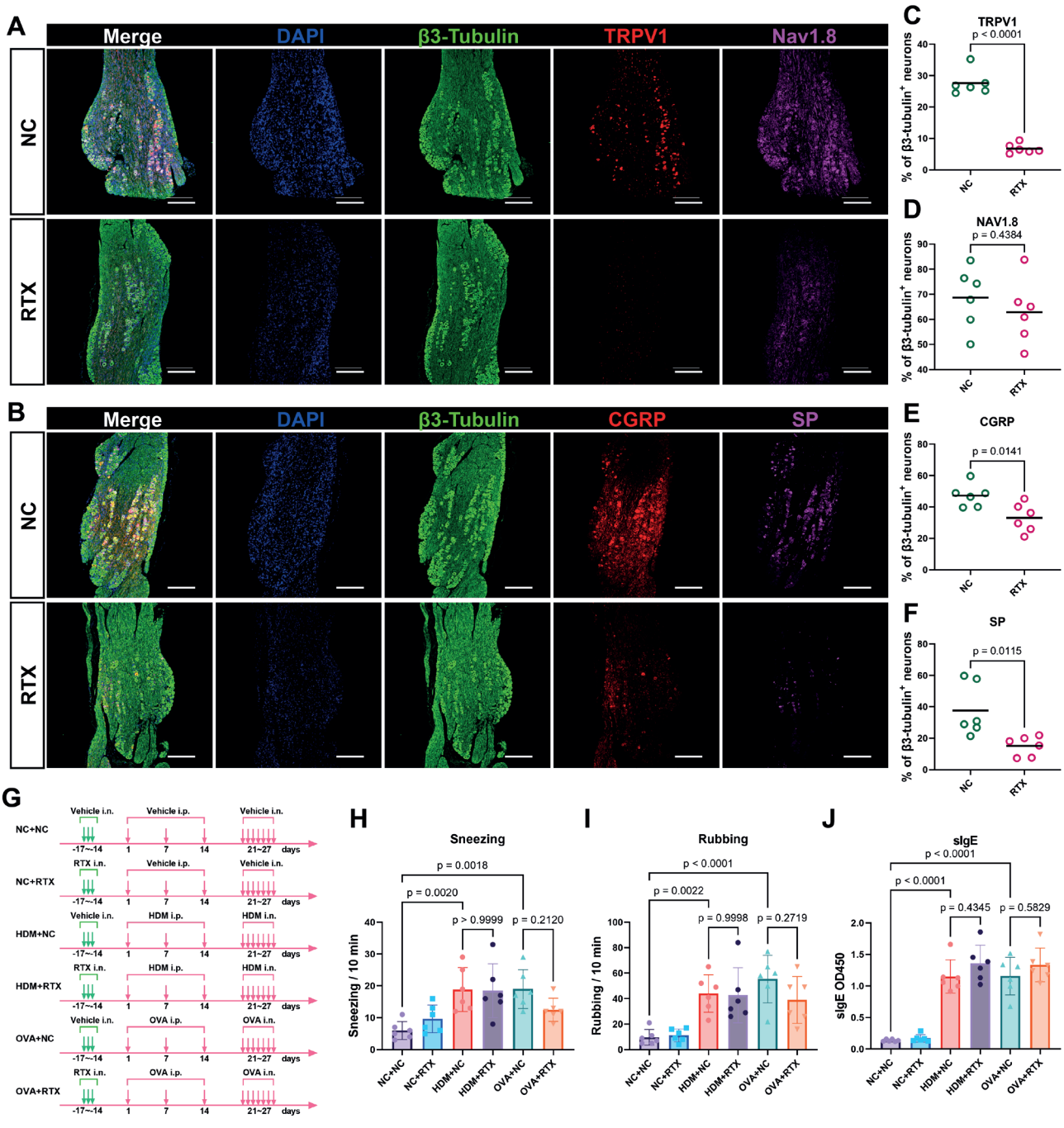

Figure 3. Resiniferatoxin (RTX)–induced silencing of trigeminal TRPV1⁺ sensory nerves. (A-B) Immunofluorescence staining for TRPV1, Nav1.8, CGRP, and SP in trigeminal ganglion neurons 6 weeks after the completion of RTX treatment. Scale bar = 250 μm. (C-F) Quantification of the proportion of neurons positive for TRPV1, Nav1.8, CGRP, and SP. (G) Schematic of the experimental timeline. Mice received RTX or vehicle, followed by a 2-week rest period before AR model induction via sensitization and challenge with HDM or OVA as described in Figure 1G. (H-I) The number of sneezes and nasal rubbing episodes recorded for 10 minutes after the final challenge. (J) Serum levels of HDM- or OVA-specific IgE (sIgE) measured by ELISA. Data for groups "NC+NC", "NC+RTX", "HDM+NC", and "HDM+RTX" show HDM-sIgE levels; data for groups "OVA+NC" and "OVA+RTX" show OVA-sIgE levels. Ordinary one-way ANOVA was used for comparisons among multiple groups, and two-sided Student's t-tests were used for comparisons between two groups. Data are presented as mean and 95% confidence interval. Abbreviations: CGRP, calcitonin gene-related peptide; SP, substance P; TRPV1, transient receptor potential vanilloid 1; Nav1.8, voltage-gated sodium channel 1.8.

Corrected Proof

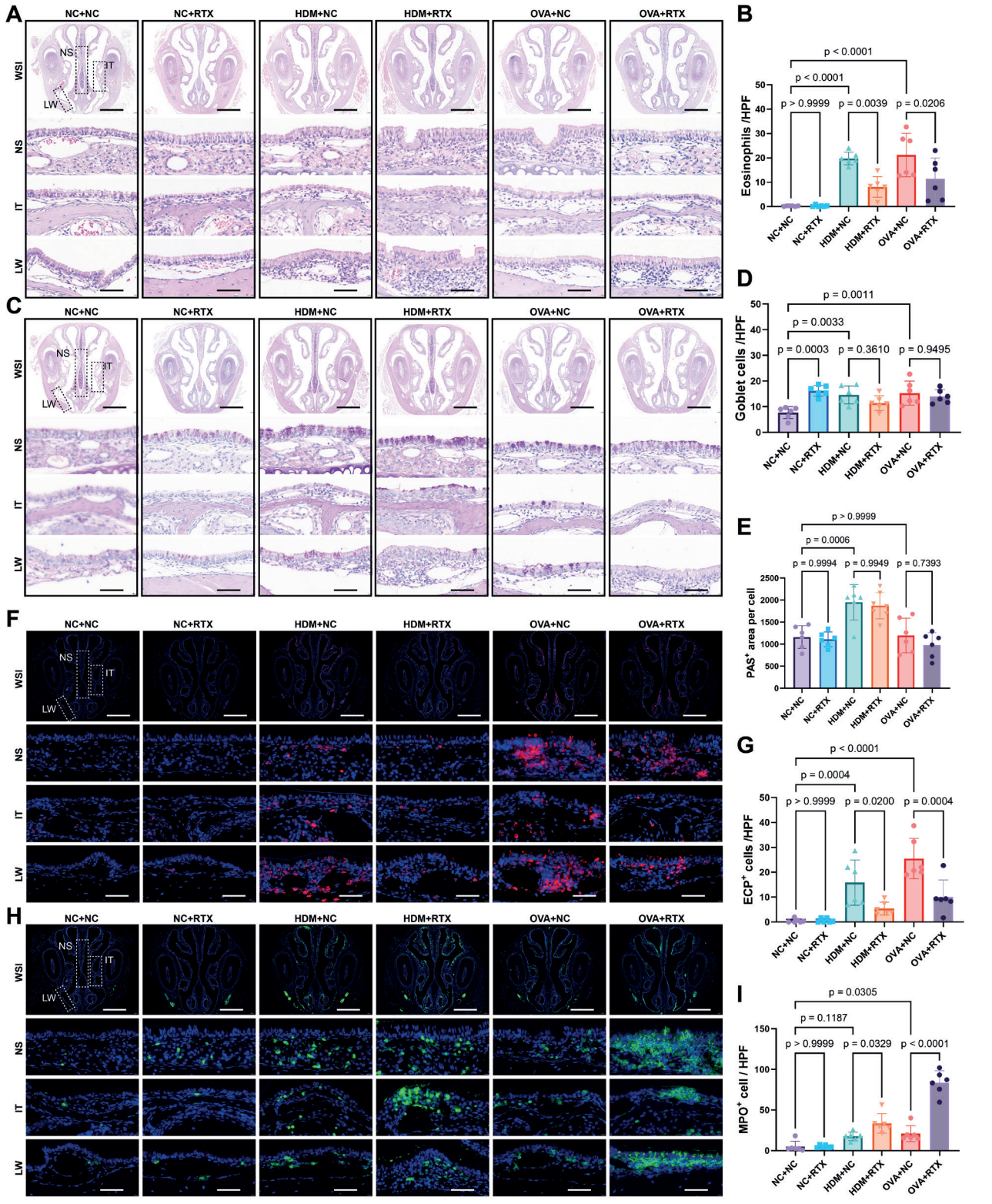

Figure 4. Silencing of TRPV1⁺ sensory neurons by RTX reduces eosinophilic but enhances neutrophilic infiltration in the nasal mucosa of AR mice. (A) Representative H&E staining of nasal mucosa and (B) quantitative analysis of eosinophil numbers. (C) PAS staining of nasal mucosa, with quantification of (D) goblet cell numbers and (E) mucin content per goblet cell. (F) Representative immunofluorescence staining for ECP and (G) quantification of ECP-positive cells. (H) Representative immunofluorescence staining for MPO and (I) quantification of MPO-positive cells. Whole-slide images (WSI) and representative images from specific anatomical regions—nasal septum (NS), inferior turbinate (IT), and lateral wall (LW)—are shown. Scale bar: 2 mm for WSI; 50 μm for other images. Ordinary one-way ANOVA was used for comparisons among multiple groups. Data are presented as mean and 95% confidence interval. Abbreviations: ECP, eosinophil cationic protein; MPO, myeloperoxidase; PAS, periodic acid-Schiff.

Corrected Proof

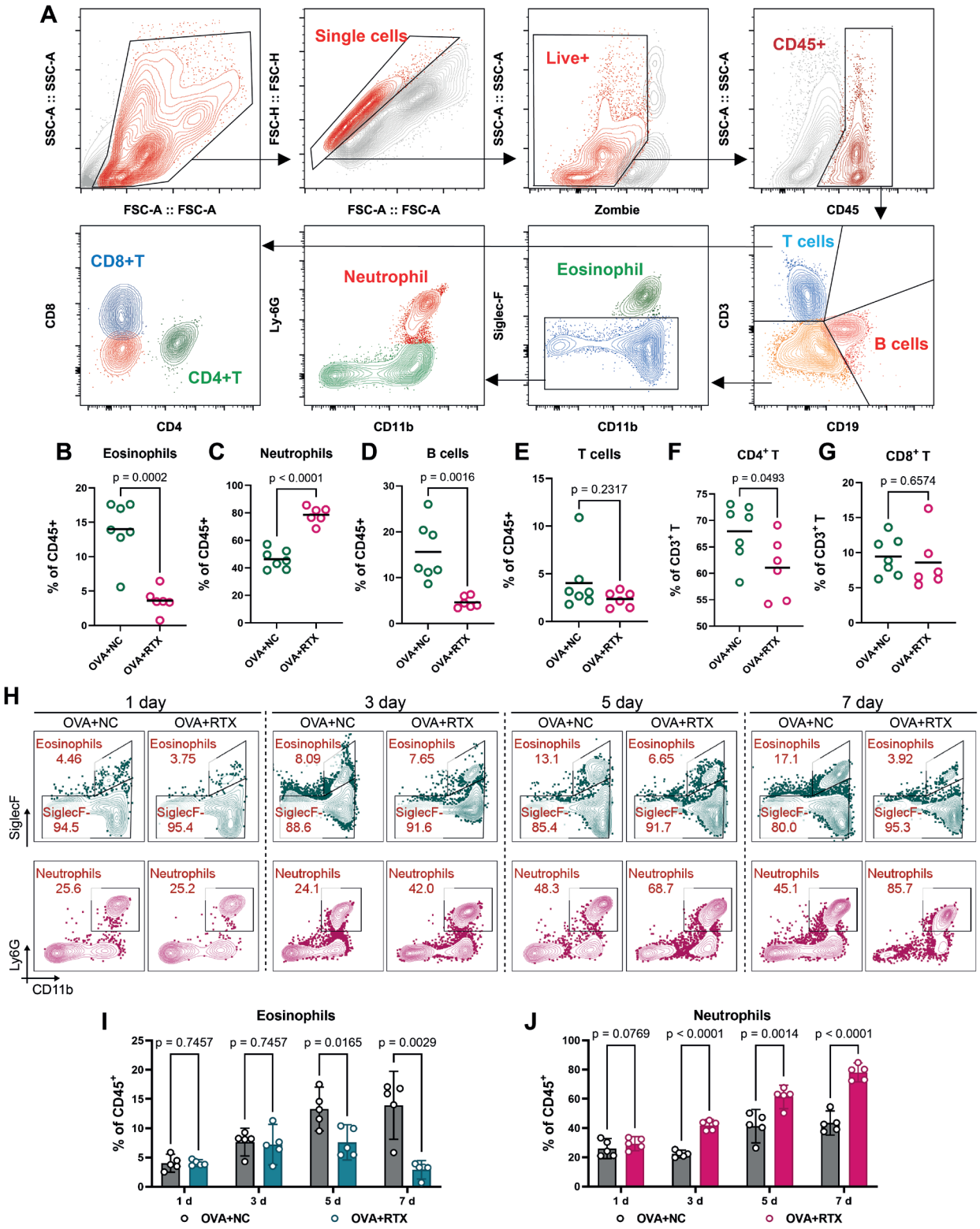

Figure 5. Flow cytometric validation of reduced eosinophilic but enhanced neutrophilic infiltration following RTX-induced silencing of TRPV1$^+$ sensory neurons in an OVA-induced model. (A) Gating strategy for distinguishing T cells (CD45$^+$CD3$^+$), CD4$^+$ T cells (CD45$^+$CD3$^+$CD4$^+$), CD8$^+$ T cells (CD45$^+$CD3$^+$CD8$^+$), B cells (CD45$^+$CD19$^+$), eosinophils (CD45$^+$CD11b$^+$Siglec-F$^+$), and neutrophils (CD45$^+$CD11b$^+$Ly6G$^+$) in the nasal mucosa. (B–G) Quantitative analysis of eosinophil, neutrophil, B cell, T cell, CD4$^+$ T cell, and CD8$^+$ T cell infiltration. (H) Representative flow cytometry plots showing eosinophil and neutrophil populations on days (d) 1, 3, 5, and 7 of continuous allergen challenge in RTX-treated and control mice. (I–J) Time-course analysis of eosinophil and neutrophil proportions in the nasal mucosa of OVA-induced AR mice following RTX or vehicle treatment. Two-sided Student's t-tests were used for comparisons in panels (B–G). For time-course data in panels (I–J), two-sided Student's t-tests with false discovery rate (FDR) correction were applied at each time point. Data are presented as mean and 95% confidence interval. Abbreviations: RTX, resiniferatoxin; d, day.

Corrected Proof

RTX-induced neutrophil increase is accompanied by exacerbated epithelial barrier damage and inflammatory burden in the AR model

To determine the changes in the neuropeptides CGRP and SP in nasal mucosal tissue following RTX-mediated silencing of TRPV1$^+$ sensory neurons, we performed immunoblotting analysis of nasal mucosal lysates. The results showed that, compared with the control group, RTX treatment significantly reduced the protein levels of CGRP and SP in the nasal mucosa of the AR model (Figures 6A, 6C, and 6D). MPO protein expression in the nasal mucosa was markedly increased after RTX treatment (Figures 6B and 6E), consistent with the immunofluorescence staining results described above.

To explore the mechanisms underlying the increased neutrophil accumulation, we measured the protein levels of CXCL1, CXCL2, and IL-17A, which are closely associated with neutrophilic inflammation [31-33], in nasal mucosal tissues. The results showed that RTX significantly upregulated CXCL2 and IL-17A protein expression in the AR model compared with the control group (Figures 6B, 6F, and 6H), suggesting that these proteins may contribute to the observed increase in neutrophils. No significant change was observed in CXCL1 levels (Figure 6G).

To clarify the impact of TRPV1$^+$ sensory neuron silencing-induced neutrophilia on epithelial barrier damage in the AR nasal mucosa, we performed immunofluorescence staining for the tight junction proteins ZO-1 and Occludin, as well as the cilia marker Acetyl-Alpha-Tubulin (Ac-α-Tub; Figure 6I). The results showed that, compared with the control group, RTX treatment significantly reduced ZO-1 and Occludin expression in the nasal epithelium of the AR model (Figures 6J and 6K), whereas Ac-α-Tub expression remained unchanged (Figure 6L). Subsequently, we detected markers of epithelial remodeling and inflammation by immunoblotting (Figures 6M and 6N). The results revealed that the basal cell markers KRT5 and P63 were significantly upregulated after RTX treatment compared with the control group (Figures 6P and 6Q). The cilia marker Ac-α-Tub showed no significant change (Figure 6O), consistent with the immunofluorescence findings. The fibroblast marker Vimentin also remained unchanged between the RTX and control groups (Figure 6R). The apoptosis marker cleaved caspase-3 (Cle-Casp3) was significantly increased in the nasal mucosa of RTX-treated AR mice (Figure 6S). Similarly, the protein expression of key pro-inflammatory mediators TNF-α, IL-1β, and IL-6 was markedly upregulated after RTX treatment compared with the control group (Figures 6T-6V). These results indicate that RTX-induced neutrophil increase is accompanied by exacerbated epithelial barrier damage, epithelial hyperplasia, and inflammatory burden in the AR model.

Discussion

The nasal cavity, as the initial segment of the respiratory tract, is densely innervated to detect environmental irritants, pathogens, and allergens. Although sensory nerve activation has been observed in AR, its immunomodulatory roles remain incompletely understood [4,6,7]. In this study, we employed pharmacological silencing of nasal TRPV1$^+$ sensory nerves to demonstrate their role in regulating inflammation in AR. We found that silencing TRPV1$^+$ sensory nerve reduced eosinophil numbers in the nasal mucosa of AR mouse models, yet concurrently promoted neutrophil infiltration. This dual effect underscores the complex and context-dependent role of sensory nerves in shaping mucosal immunity.

Our experimental results indicate that inhibiting sensory nerve signaling significantly reduces eosinophilic infiltration in the nasal mucosa of AR mice. This finding aligns with growing evidence implicating sensory nerves in type 2 inflammation in allergic airway diseases [34-38]. Specifically, silencing nociceptive neurons (e.g., Nav1.8$^+$ neurons) effectively attenuates type 2 allergic airway inflammation [35]. Upon activation, sensory nerves release neuropeptides, including substance P (SP) and calcitonin gene-related peptide (CGRP), which can directly or indirectly promote the recruitment and activation of eosinophils—key effector cells in AR pathogenesis [39]. Thus, the observed reduction in eosinophils in our model may reasonably be attributed to decreased release of these pro-inflammatory neuropeptides following sensory nerve blockade.

Unexpectedly, we observed a marked increase in neutrophils upon sensory nerve inhibition. Further time-course analysis revealed that in the RTX-treated OVA-induced model, neutrophilic expansion was detected as early as day 3 of consecutive challenge, preceding the significant reduction in eosinophils observed on day 5. This chronological sequence suggests that neutrophilia is not merely a compensatory response secondary to eosinophil loss, but rather a direct immunological consequence of neuronal silencing. Notably, a recent study using a model of allergic contact dermatitis similarly found that selective ablation of TRPV1$^+$ peptidergic neurons resulted in significantly increased neutrophilic infiltration and aggravated tissue damage in the skin [40]. This parallel finding suggests that the negative regulation of neutrophilic inflammation by TRPV1$^+$ sensory nerves may represent a cross-organ neuroimmune mechanism.

To explore the underlying mechanisms, we examined the expression of neuropeptides and neutrophil-associated factors in nasal mucosal tissues. RTX treatment significantly decreased protein levels of CGRP and SP in the nasal mucosa, concomitant with pronounced upregulation of the neutrophil chemoattractant CXCL2 and the cytokine IL-17A. Previous studies have demonstrated that CGRP can directly suppress neutrophil migration toward chemokines via the RAMP1 receptor, accelerate neutrophil apoptosis within the inflammatory microenvironment, and enhance macrophage efferocytosis, thereby limiting neutrophil accumulation in tissues [41,42]. Thus, the loss of CGRP

Corrected Proof

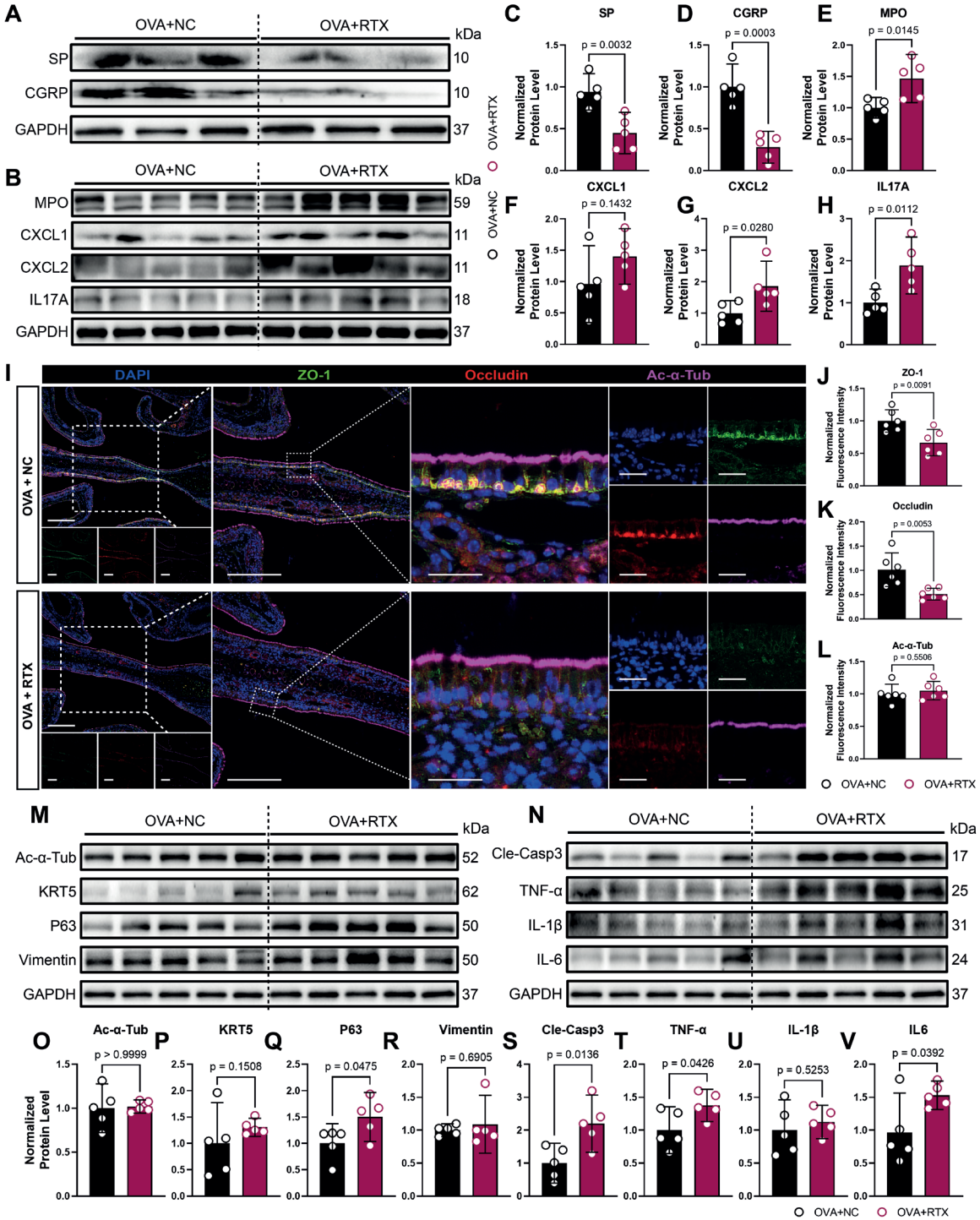

Figure 6. RTX-induced neutrophil increase is accompanied by exacerbated epithelial barrier damage and inflammatory burden in the AR model. (A) Representative western blot images and (C–D) quantification of CGRP and SP protein levels in nasal mucosal lysates from control and RTX-treated AR mice. (B) Representative western blot images and (E–H) quantification of MPO, CXCL1, CXCL2, and IL-17A protein levels. (I) Representative immunofluorescence staining for ZO-1, Occludin, and Acetyl-α-Tubulin (Ac-α-Tub) in nasal mucosa sections. Scale bars: 250 μm for the first and second columns; 25 μm for the third, fourth, and fifth columns. (J–L) Quantification of ZO-1, Occludin, and Ac-α-Tub fluorescence intensity normalized to basement membrane length. (M–N) Representative western blot images and (O–V) quantification of Ac-α-Tub, KRT5, P63, Vimentin, cleaved caspase-3 (Cle-Casp3), TNF-α, IL-1β, and IL-6 protein levels in nasal mucosal lysates. GAPDH was used as loading control. Two-sided Student's t-tests were used for comparisons between two groups. Data are presented as mean and 95% confidence interval. Abbreviations: Ac-α-Tub, acetyl-α-tubulin; CGRP, calcitonin gene-related peptide; Cle-Casp3, cleaved caspase-3; CXCL, C-X-C motif chemokine ligand; DAPI, 4',6-diamidino-2-phenylindole; GAPDH, glyceraldehyde-3-phosphate dehydrogenase; IL, interleukin; KRT5, keratin 5; MPO, myeloperoxidase; RTX, resiniferatoxin; SP, substance P; TNF-α, tumor necrosis factor alpha; ZO-1, zonula occludens-1.

Corrected Proof

following TRPV1+ neuron ablation may relieve these inhibitory constraints on neutrophil activity. In addition, nociceptor-derived VIP and SST may similarly contribute to the observed neutrophilia. Vasoactive intestinal peptide (VIP) inhibits NF-κB-dependent production of CXCL8 and CXC chemokines via VPAC1 signaling, thereby attenuating neutrophil chemotaxis [43,44]. Somatostatin (SST), released from sensory nerve endings upon activation, directly suppresses neutrophil infiltration through SSTR5 [45]. Moreover, the upregulation of IL-17A, a key mediator of neutrophil mobilization and activation [31], further indicates that the local immune milieu undergoes remodeling in the absence of sensory neuropeptides, thereby amplifying neutrophil recruitment signals. Collectively, the increased neutrophilia observed after TRPV1+ neuron ablation likely reflects the combined loss of multiple neuropeptide signals and the consequent reshaping of the local immune microenvironment.

Notably, the increase in neutrophils was accompanied by exacerbated epithelial barrier damage in the nasal mucosa. In RTX-treated AR mice, expression of the tight junction proteins ZO-1 and Occludin was significantly reduced, while markers of basal cell hyperplasia (KRT5 and P63) and apoptosis (cleaved caspase-3) were elevated. Furthermore, the release of pro-inflammatory cytokines, including TNF-α, IL-1β, and IL-6, was markedly increased. These findings indicate that the neutrophil-predominant inflammation induced by TRPV1+ neuron ablation is not merely a shift in cellular composition but is associated with aggravated tissue injury and an elevated overall inflammatory burden.

A noteworthy observation in this study is the differential effect on behavioral symptoms: QX-314 treatment significantly alleviated allergen-induced sneezing and nasal rubbing, whereas RTX treatment, despite near-complete ablation of TRPV1+ neurons, failed to ameliorate these responses. QX-314 is a positively charged lidocaine derivative whose cellular entry depends on the opening of TRP channels; once inside, it blocks Nav1.8 voltage-gated sodium channels, thereby inhibiting action potential generation and propagation [15,16]. The transcription and synthesis of neuropeptides in sensory neuron somata are governed by activity-dependent calcium signaling pathways: depolarization-induced calcium influx promotes CGRP gene expression through activation of Ca^{2+}/calmodulin-dependent protein kinase (CaMK) and cAMP response element-binding protein (CREB), whereas blockade of neuronal electrical activity downregulates this pathway [46]. In contrast, RTX is an ultrapotent TRPV1 agonist that induces sustained calcium influx, leading to irreversible excitotoxic injury and ablation of TRPV1-expressing neurons [19]. Multiplex immunofluorescence of trigeminal ganglia revealed that RTX markedly reduced the number and activation (p-ERK1/2) of TRPV1+ and SST+ neurons, but induced a compensatory increase in the proportion and activation of TRPA1+ neurons; activation of HRH1+ neurons was also elevated. TRPA1 mediates sneezing [27], and HRH1+ neurons are linked to histamine-induced pruritus [28]. QX-314 did not alter the proportions of these subsets but, under inflammatory conditions, entered a broader range of neurons through activated TRP channels [15,35], suppressing activation of TRPV1+, TRPA1+, and HRH1+ neurons. These findings suggest that TRPV1 ablation alone is insufficient to suppress AR symptoms due to compensatory pathways (TRPA1, HRH1), indicating functional redundancy. The superior symptomatic relief by QX-314 likely reflects its broader inhibitory effect across multiple symptom-relevant neuronal subsets.

Flow cytometric analysis further revealed a significant reduction in CD19+ B cells within the nasal mucosa following RTX treatment. This observation is consistent with previous reports demonstrating that sensory neuron depletion leads to decreased B cell numbers and impaired antibody production [47]. Mathur and colleagues further showed that substance P released by nociceptors directly triggers IgE class switching in B cells [48], whereas Wu and colleagues found that spleen-innervating nociceptors promote germinal center responses and humoral immunity through the release of CGRP [49]. In the present study, RTX treatment concomitantly reduced protein levels of both CGRP and SP in the nasal mucosa, suggesting that the diminished B cell infiltration may result from the simultaneous loss of multiple neuropeptide signals. Thus, the diminished B cell infiltration observed here likely reflects the combined loss of these neuropeptide signals. Further investigation is warranted to clarify the precise contribution of distinct neuropeptides to local B cell regulation in the AR nasal mucosa.

The central finding of this study is that silencing TRPV1-expressing sensory nerves alleviates eosinophilic infiltration but shifts the inflammatory response toward neutrophilic predominance in the nasal mucosa of AR models. The clinical implications of these findings are twofold. Firstly, they support the therapeutic rationale of targeting neuronal pathways to alleviate type 2 inflammation in AR. However, secondly, the reciprocal increase in neutrophils reveals a potential limitation of broad-spectrum sensory nerve inhibition. This compensatory mechanism may explain why some clinical trials targeting specific neuronal pathways, such as with the TRPV1 antagonist SB-705498, have yielded limited success [50]. Our results suggest that future translational efforts should aim for more precise neuromodulation, potentially by targeting specific neuropeptide receptors or by developing strategies that concurrently manage both neural hyperactivity and the resultant neutrophil-predominant inflammation to achieve optimal therapeutic outcomes.

Conclusion

Our study demonstrates that silencing nasal TRPV1+ sensory nerves exerts a dual effect on allergic rhinitis: it ameliorates type 2 inflammation by reducing eosinophil infiltration, but paradoxically promotes neutrophilic inflammation. This shift underscores

Corrected Proof

the critical role of sensory nerves in maintaining immune balance and highlights a significant limitation of broad-spectrum neuromodulation. Future therapeutic strategies should therefore aim for more precise targeting of specific neuro-immune pathways to achieve optimal control of allergic inflammation without triggering compensatory neutrophil responses.

Acknowledgments

The authors wish to express their sincere gratitude to the staff at the Medical Research Center of the Third Affiliated Hospital of Sun Yat-sen University for their expert technical guidance. We also extend our thanks to all laboratory members for their stimulating discussions and constructive input.

Author contributions

FY, YT, and JC: These authors contributed equally to this work. FY, YT, and JC RW and YL: Participated in investigation, validation, and data curation. ZS and QY: As the corresponding author, oversaw conceptualization, acquired funding, administered the project, and was responsible for writing – review & editing, and final approval of the manuscript.

Conflict of interest

The authors declare no conflicts of interest.

Funding

This work was supported by National Key R&D Program of China (2022YFC2504100), The National Natural Science Foundation of China (U20A20399; 82171114), The Key-area Research and Development Programme of Guangdong Province (2020B0101130015), The General Program of Natural Science Foundation of Guangdong Province (2021A1515011764), Sun Yat-sen University Clinical Research 5010 Program (2019006), and The Third Affiliated Hospital of Sun Yat-sen University "Five by Five" Project (2023ww601).

References

1. Kim B, Rothenberg ME, Sun X, et al. Neuroimmune interplay during type 2 inflammation: Symptoms, mechanisms, and therapeutic targets in atopic diseases. J Allergy Clin Immunol. 2024;153(4):879-93.
2. Undem BJ, Taylor-Clark T. Mechanisms underlying the neuronal-based symptoms of allergy. J Allergy Clin Immunol. 2014;133(6):1521-34.
3. Velasco E, Delicado-Miralles M, Hellings PW, Gallar J, Van Gerven L, Talavera K. Epithelial and sensory mechanisms of nasal hyperreactivity. Allergy. 2022;77(5):1450-63.
4. Backaert W, Steelant B, Wils T, et al. Nasal hyperreactivity in allergic rhinitis and chronic rhinosinusitis with polyps: a role for neuronal pathways. Rhinology. 2024;62(3):299-309.
5. Chiu IM, Sokol CL. Neuroimmune recognition of allergens. Curr Opin Immunol. 2024;90:102458.
6. Keh SM, Facer P, Simpson KD, Sandhu G, Saleh HA, Anand P. Increased nerve fiber expression of sensory sodium channels Nav1.7, Nav1.8, And Nav1.9 in rhinitis. Laryngoscope. 2008;118(4):573-9.
7. O'Hanlon S, Facer P, Simpson KD, Sandhu G, Saleh HA, Anand P. Neuronal markers in allergic rhinitis: expression and correlation with sensory testing. Laryngoscope. 2007;117(9):1519-27.
8. Han P, Messou M, Ajit J, von Andrian UH. Setting the tone: nociceptors as conductors of immune responses. Trends Immunol. 2024;45(10):783-98.
9. Zhang W, Lyu M, Bessman NJ, et al. Gut-innervating nociceptors regulate the intestinal microbiota to promote tissue protection. Cell. 2022;185(22):4170-89.
10. Barilla RM, Berard C, Sun L, , et al. Type 2 cytokines act on enteric sensory neurons to regulate neuropeptide-driven host defense. Science. 2025;389(6757):260-7.
11. Zhu Y, Meerschaert KA, Galvan-Pena S, et al. A chemogenetic screen reveals that Trpv1-expressing neurons control regulatory T cells in the gut. Science. 2024;385(6708):eadk1679.
12. Hou Y, Sun L, LaFleur MW, et al. Neuropeptide signalling orchestrates T cell differentiation. Nature. 2024;635(8038):444-52.
13. Xu H, Guo L, Hao T, et al. Nasal solitary chemosensory cells govern daily rhythm in mouse model of allergic rhinitis. J Allergy Clin Immunol. 2024;154(3):707-18.
14. Ryu J, Yoo J, Kim M, et al. Distinct TLR-mediated pathways regulate house dust mite-induced allergic disease in the upper and lower airways. J Allergy Clin Immunol. 2013;131(2):549-61.
15. Ito K, Kanemitsu Y, Ueda T, Kamiya T, Kubota E, Mori Y, et al. Comorbid functional dyspepsia reflects IL-33-mediated airway neuronal dysfunction in asthma. J Allergy Clin Immunol.. 2024;154(6):1422-33.
16. Binshtok AM, Bean BP, Woolf CJ. Inhibition of nociceptors by TRPV1-mediated entry of impermeant sodium channel blockers. Nature. 2007;449(7162):607-10.
17. Jiang H, Cui H, Chen M, et al. Divergent sensory pathways of sneezing and coughing. Cell. 2024;187(21):5981-97.
18. Kim HY, Kim K, Li HY, et al. Selectively targeting pain in the trigeminal system. Pain. 2010;150(1):29-40.
19. Li F, Jiang H, Shen X, et al. Sneezing reflex is mediated by a peptidergic pathway from nose to brainstem. Cell. 2021;184(14):3762-73.
20. Almanzar N, Yang D, Xia J, et al. Vagal TRPV1(+) sensory neurons protect against influenza virus infection by regulating lung myeloid cell dynamics. Science Immunol. 2025;10(110):eads6243.
21. Lin J, Chen D, Guan L, et al. House dust mite exposure enhances immune responses to ovalbumin-induced intestinal allergy. Sci Rep. 2022;12(1):5216.
22. Bystrom J, Amin K, Bishop-Bailey D. Analysing the eosinophil cationic protein--a clue to the function of the eosinophil granulocyte. Resp Res. 2011;12(1):10.
23. Venge P. Monitoring the allergic inflammation. Allergy. 2004;59(1):26-32.
24. Klebanoff SJ. Myeloperoxidase: friend and foe. J Leukocyte Biol. 2005;77(5):598-625.
25. Wang B, Jiang B, Li G, et al. Somatosensory neurons express specific sets of lincRNAs, and lincRNA CLAP promotes itch sensation in mice. EMBO R. 2023;24(2):e54313.
26. Grundy L, Caldwell A, Garcia Caraballo S, et al. Histamine induces peripheral and central hypersensitivity to bladder distension via the histamine H(1) receptor and TRPV1. American journal of physiology. Renal Physiol. 2020;318(2):F298-314.
27. Fang Z, Yi F, Peng Y, et al. Inhibition of TRPA1 reduces airway inflammation and hyperresponsiveness in mice with allergic rhinitis. FASEB J. 2021;35(5):e21428.
28. Xing Y, Steele HR, Hilley HB, et al. Visualizing the itch-sensing skin arbors. J Invest Dermatol. 2021;141(5):1308-16.
29. Bolden JE, Lucas EC, Zhou G, et al. Identification of a Siglec-F+ granulocyte-macrophage progenitor. J Leukocyte Biol. 2018;104(1):123-33.
30. Ghasemlou N, Chiu IM, Julien J, Woolf CJ. CD11b+Ly6G- myeloid cells mediate mechanical inflammatory pain hypersensitivity. Proc Natl Acad Sci. 2015;112(49):E6808-17.
31. Bae JS, Kim JH, Kim EH, Mo JH. The role of IL-17 in a lipopolysaccharide-induced rhi-

Corrected Proof

nitis model. Allergy, Asthma Immunol Res. 2017;9(2):169-76.
32. Kim EH, Kim JH, Samivel R, et al. Intralymphatic treatment of flagellin-ovalbumin mixture reduced allergic inflammation in murine model of allergic rhinitis. Allergy. 2016;71(5):629-39.
33. Cardoso C, Carvalho ANFS, Lara ESN, et al. Plasmin modulates neutrophilic inflammation and alveolar macrophage function, protecting mice from Pneumococcal pneumonia. Blood. 2026:2025028733.
34. Crosson T, Wang J, Doyle B, et al. FcεR1-expressing nociceptors trigger allergic airway inflammation. J Allergy Clin Immunol. 2021 2021-6-1;147(6):2330-42.
35. Talbot S, Abdulnour RE, Burkett PR, et al. Silencing Nociceptor Neurons Reduces Allergic Airway Inflammation. Neuron. 2015;87(2):341-54.
36. Balestrini A, Joseph V, Dourado M, et al. A TRPA1 inhibitor suppresses neurogenic inflammation and airway contraction for asthma treatment. J Exp Med. 2021;218(4):e20201637.
37. Bao C, Abraham SN. Mast cell-sensory neuron crosstalk in allergic diseases. J Allergy Clin Immunol. 2024;153(4):939-53.
38. Matsuo Y, Yanase Y, Irifuku R, et al. Neuromedin U directly induces degranulation of skin mast cells, presumably via MRGPRX2. Allergy. 2018;73(11):2256-60.
39. Fang Z, Fu Y, Yi F, et al. Neural control of the pathophysiology of allergic airway disease and its clinical implications: a focus on allergic rhinitis and asthma. J Allergy Clin Immunol. 2025;156(2):259-69.
40. Voisin T, Gheziel N, El Samrout C, et al. Skin inflammation and itch response are independently regulated by distinct nociceptor subsets. Immunity. 2026. 59,5P1237-1252.E9
41. Lu Y, Nayer B, Singh SK, et al. CGRP sensory neurons promote tissue healing via neutrophils and macrophages. Nature. 2024;628(8008):604-11.
42. Baral P, Umans BD, Li L, et al. Nociceptor sensory neurons suppress neutrophil and γδ T cell responses in bacterial lung infections and lethal pneumonia. Nat Med. 2018;24(4):417-26.
43. Delgado M, Jonakait GM, Ganea D. Vasoactive intestinal peptide and pituitary adenylate cyclase-activating polypeptide inhibit chemokine production in activated microglia. Glia. 2002;39(2):148-61.
44. Delgado M, Ganea D. Vasoactive intestinal peptide inhibits IL-8 production in human monocytes by downregulating nuclear factor kappaB-dependent transcriptional activity. Biochem Biophys Res Commun. 2003 2003-3-7;302(2):275-83.
45. Chen X, Li Y, Lu L, et al. Activation of the SST-SSTR5 signaling pathway enhances corneal wound healing in diabetic mice. Mucosal Immunol. 2024;17(5):858-70.
46. Nakanishi M, Hata K, Nagayama T, et al. Acid activation of Trpv1 leads to an up-regulation of calcitonin gene-related peptide expression in dorsal root ganglion neurons via the CaMK-CREB cascade: a potential mechanism of inflammatory pain. Mol Biol Cell. 2010;21(15):2568-77.
47. Aguilar D, Zhu F, Millet A, et al. Sensory neurons regulate stimulus-dependent humoral immunity in mouse models of bacterial infection and asthma. Nat Commun. 2024;15(1):8914.
48. Mathur S, Wang J, Seehus CR, et al. Nociceptor neurons promote IgE class switch in B cells. JCI insight. 2021;6(24):e148510.
49. Wu M, Song G, Li J, , et al. Innervation of nociceptor neurons in the spleen promotes germinal center responses and humoral immunity. Cell. 2024;187(12):2935-51.
50. Alenmyr L, Greiff L, Andersson M, Sterner O, Zygmunt PM, H Gest Tt ED. Effect of mucosal TRPV1 inhibition in allergic rhinitis. Basic Clin Pharmacol. 2012;110(3):264-8.

Zhaohui Shi, MD, PhD
Department of Otolaryngology
Head and Neck Surgery
The Third Affiliated Hospital of Sun Yat-sen University
No. 600 Tianhe Road
Tianhe District
Guangzhou 510630
China

Tel: +86 20-85252239
E-mail: shizhh35@mail.sysu.edu.cn

Qintai Yang, MD, PhD
Department of Otolaryngology

Tel: +86 20-85252239
E-mail: yangqint@mail.sysu.edu.cn

Fan Ye*[,1,3,5], Ying Tao*[,2], Junhai Chen*[,1,3,5], Ruizhi Wang[1,3,5], Yiwen Li[1,3,5], Zhaohui Shi[1,3,4,5], Qintai Yang[1,3,4,5]

[1] Department of Otolaryngology-Head and Neck Surgery, The Third Affiliated Hospital of Sun Yat-Sen University, Guangzhou, China
[2] Department of Otolaryngology-Head and Neck Surgery, Shenzhen Third People's Hospital, Shenzhen, China
[3] Department of Allergy, The Third Affiliated Hospital of Sun Yat-Sen University, Guangzhou, China
[4] Naso-Orbital-Maxilla and Skull Base Center, The Third Affiliated Hospital of Sun Yat-Sen University, Guangzhou, China
[5] Key Laboratory of Airway Inflammatory Disease Research and Innovative Technology Translation, Guangzhou, China

* contributed equally

Rhinology 64: 5, 0 - 0, 2026
https://doi.org/10.4193/Rhin25.667

Received for publication:
October , 2025
Accepted: May 16, 2026

Associate Editor:
Michael Soyka

This manuscript contains online supplementary material

Corrected Proof

SUPPLEMENTARY MATERIAL

Materials and Methods

Animals and allergic rhinitis models

All BALB/c mice were purchased from the Guangdong Provincial Experimental Animal Center and housed in a specific pathogen-free (SPF) facility. Mice used in all experiments were aged between 6 and 12 weeks, matched for sex and age prior to experiments, and maintained under a 12-hour light-dark cycle with free access to food and water. All experimental protocols were approved by the Institutional Animal Care and Use Committee (IACUC) of Sun Yat-Sen University (Approval No. SYSU-IACUC-2025-B2045).

To establish house dust mite (HDM) or ovalbumin (OVA)-induced murine models of allergic rhinitis (Figures 1G and 3G), mice were sensitized via intraperitoneal (i.p.) injection of 200 µL saline containing either 100 µg HDM extract (Cat# XPB82D3A2.5, Greer labs) or 50 µg OVA (Cat# A5503, Sigma-Aldrich) adsorbed to 2 mg aluminum hydroxide (Cat# KX0210054, Biodragon) on days 0, 7, and 14. From days 21 to 27, nasal inflammation was elicited by intranasal administration of 10 µL (5 µL/nostril) saline containing 50 µg HDM protein or 1 mg OVA without anesthesia [1,2]. Unless otherwise specified, control mice received i.p. injections or intranasal instillations of an equivalent volume of saline. After the final intranasal challenge, videos were recorded and analyzed by an investigator blinded to the experimental groups to count the number of sneezes and nasal rubbings.

Silencing of nasal sensory nerves with QX-314 or resiniferatoxin (RTX)

QX-314, a positively charged lidocaine derivative, acts as a sodium channel blocker that inhibits the activity of Nav1.8-expressing nociceptive neurons [3,4]. Its entry into neurons is dependent on the opening of TRP channels [3,4]. To inhibit TRPV1-expressing sensory nerves, a mixture of 10 µL capsaicin (a TRPV1 receptor agonist; 1 µM, Cat# No. 0462, Tocris) and 1% QX-314 (Cat# 552233, Sigma-Aldrich) was administered intranasally [4-6]. This mixture was given 1 hour before each nasal allergen challenge. The control group received an equal volume of 0.9% saline containing 1% (v/v) DMSO. RTX, a potent TRPV1 agonist, induces irreversible neuronal depolarization [7]. Mice received intranasal RTX (Cat# GC12783, GlpBio) in an escalating dose regimen (30, 70, and 100 µg/kg) over three consecutive days [7,8], followed by a 14-day rest period before subsequent experiments. Control mice for this experiment were treated with an equal volume of 0.9% saline containing 1% (v/v) DMSO.

Enzyme-Linked Immunosorbent Assay (ELISA)

Serum levels of HDM- and OVA-specific IgE were quantified by ELISA as described previously [9]. In brief, 96-well plates were coated overnight at 4°C with 100 µL of HDM (1 µg/well) or OVA (10 µg/well) in carbonate-buffered saline (CBS, pH 9.5). Following three washes with PBST (PBS containing 0.05% Tween 20), the plates were blocked with 3% BSA in PBS for 1 h at 37°C. Subsequently, wells were incubated for 2 h at 37°C with serum samples diluted 1:5 in the blocking buffer, followed by a 2 h incubation with HRP-conjugated goat anti-mouse IgE (1:2000, Invitrogen, Cat# SA5-10263). After a final wash, the color reaction was developed with TMB substrate for 20 min and terminated with 2 M H_2SO_4. Absorbance was read at 450 nm using a microplate reader (BioTek).

Histology

Nasal tissues were fixed in 4% paraformaldehyde for 24 hours at room temperature. After rinsing with PBS, tissues were decalcified in EDTA solution for 3 weeks, with the decalcification solution replaced weekly. Tissues were then embedded in paraffin and serially sectioned into 4-µm thick slices. Sections were deparaffinized in xylene, rehydrated through a graded ethanol series, and rinsed in distilled water. For hematoxylin and eosin (H&E) staining, rehydrated sections were stained with hematoxylin for 5 minutes to visualize nuclear structures, differentiated in 1% acid alcohol for a few seconds, and blued in running water. This was followed by counterstaining with eosin for 1 minute. After staining, sections were dehydrated, cleared in xylene, and mounted with neutral balsam. For periodic acid-Schiff (PAS) staining, sections were sequentially oxidized with 0.5% periodic acid for 10 minutes, rinsed with distilled water, incubated with Schiff's reagent in the dark for 5 minutes, and then counterstained with hematoxylin for nuclei. Finally, sections were dehydrated, cleared, and mounted with neutral balsam. Images were acquired using a whole-slide scanner.

Immunofluorescence

For immunofluorescence staining, nasal and trigeminal ganglion sections were first deparaffinized, rehydrated, and subjected to antigen retrieval via heat induction in Tris-EDTA buffer (95°C, 20 min). After quenching endogenous peroxidases with 3% H_2O_2 (15 min) and blocking with 10% goat serum (1 h, RT), the sections were incubated with primary antibodies at 4°C overnight. The following primary antibodies were used: mouse anti-β3-Tubulin (1:1000, Cat# ab78078, Abcam), rabbit anti-TRPV1 (1:500, Cat# ab305299, Abcam), mouse anti-Nav1.8 (1:500, Cat# 75-166, NeuroMab), mouse anti-CGRP (1:500, Cat# ab81887, Abcam), rat anti-SP (1:100, Cat# sc-21715, Santa Cruz), rabbit anti-NeuN (1:500, Cat# ab177487, Abcam), rabbit

Corrected Proof

anti-Somatostatin (1:500, Cat# 72602, CST), rabbit anti-TRPA1 (1:500, Cat# NB110-40763, Novus), rabbit anti-HRH1 (1:500, Cat# 28763-1-AP, Proteintech), rabbit anti-p-ERK1/2 (1:500, Cat# 4695, CST), rabbit anti-ECP (1:500, Cat# 99106, CST), rabbit anti-MPO (1:1000, Cat# ab208670, Abcam), rabbit anti-ZO-1 (1:500, Cat# 21773-1-AP, Proteintech), rabbit anti-Occludin (1:200, Cat# ab216327, Abcam), and rabbit anti-Acetyl-alpha Tubulin (1:1000, Cat# ab24610, Abcam). After PBS washes, sections were probed with corresponding HRP-conjugated secondary antibodies (1:500, Invitrogen) for 1 h at RT, followed by signal amplification with Fluorescein-, CY3-, or CY5-tyramide TSA reagents (5 min in dark, AAT Bioquest). Finally, nuclei were counterstained with DAPI, and slides were mounted with Fluoromount-G (Southern Biotech) for imaging under a Nikon microscope or a whole-slide scanner.

Histological and immunofluorescence image analysis

Unless otherwise specified, high-power field images of anatomical regions such as the nasal septum, inferior turbinate, and lateral nasal wall mucosa were analyzed. For H&E-stained sections, eosinophils were counted, and the average number per high-power field was calculated. For PAS-stained sections, ImageJ software was used to quantify the PAS-positive area within the epithelial region under a uniform threshold. The PAS-positive area per goblet cell was calculated by dividing the total epithelial PAS-positive area by the number of goblet cells. For ECP and MPO staining, positive cells were counted, and the average number per high-power field was determined.

For multiplex fluorescence analysis of the trigeminal ganglion, we used QuPath software (version 0.60; https://qupath.github.io) following the software's instructions. Briefly, neuronal somata were segmented and detected based on NeuN-positive regions. Subsequently, under consistent threshold settings, other fluorescence channels were classified as positive or negative (representative images are shown in Figure S1A and S1B). Finally, the classification results from all fluorescence channels were merged to determine the combination of markers expressed by each neuronal soma.

Western blotting

Nasal mucosal tissues were lysed in RIPA buffer containing protease and phosphatase inhibitors. Protein concentrations were determined using a BCA assay. Equal amounts of protein (10-20 μg per lane) were separated by SDS-PAGE and transferred onto PVDF membranes. Membranes were blocked with a rapid blocking buffer for 15 min at room temperature, then incubated overnight at 4°C with the following primary antibodies: rabbit anti-CGRP (1:1000, Cat# 14959, CST), rabbit anti-SP (1:1000, Cat# DF7522-50, Affinity Biosciences), rabbit anti-MPO (1:2500, Cat# ab208670, Abcam), rabbit anti-CXCL1 (1:1000, Cat# ab322200, Abcam), rabbit anti-CXCL2 (1:1000, Cat# 26791-1-AP, Proteintech), rabbit anti-IL-17A (1:1000, Cat# ab79056, Abcam), rabbit anti-KRT5 (1:1000, Cat# ab79056, Abcam), rabbit anti-P63 (1:1000, Cat# ab124762, Abcam), rabbit anti-P63 (1:1000, Cat# ab124762, Abcam), rabbit anti-cleaved caspase-3 (1:1000, Cat# 9664, CST), rabbit anti-TNF-α (1:1000, Cat# 17590-1-AP, Proteintech), rabbit anti-IL-1β (1:1000, Cat# 16806-1-AP, Proteintech), rabbit anti-IL-6 (1:1000, Cat# 26404-1-AP, Proteintech), rabbit anti-IL-6 (1:1000, Cat# 26404-1-AP, Proteintech), Mouse anti-GAPDH (1:1000, Cat# 60004-1-Ig, Proteintech). After washing, membranes were incubated with HRP-conjugated secondary antibodies for 1 h at room temperature. Protein bands were visualized using enhanced chemiluminescence (Cat# 1705062, BIO-RAD) and imaged with a chemiluminescence detection system. Band intensities were quantified using ImageJ software and normalized to the loading control.

Flow cytometry of nasal mucosa

The nasal mucosa was carefully dissected and placed in HBSS containing 5% FBS on ice. Tissues were minced and enzymatically digested using a mixture of 2 mg/mL collagenase II (Cat# 17101015, Invitrogen), 1 mg/mL dispase (Cat# D4693, Sigma), and 0.2 mg/mL DNase I (Cat# 10104159001, Roche) in HBSS with 5% FBS, incubated at 37°C with shaking for 30 minutes. The cell suspension was filtered through a 70-μm strainer and centrifuged at 350g for 5 minutes. The pellet was resuspended in red blood cell lysis buffer, incubated on ice for 5 minutes, washed with an equal volume of PBS, and centrifuged to obtain a single-cell suspension.

Cells were first stained with Zombie Aqua (1:500, Cat# 423104, BioLegend) on ice for 20 minutes. After washing with cell staining buffer (Cat# 420201, BioLegend), cells were blocked using Mouse TruStain Fc Block (1:100, Cat# 156603, BioLegend) and stained with different antibody cocktails in staining buffer for 30 minutes on ice. The antibodies used included: FITC anti-mouse CD45 (clone 30-F11, 1:100, Cat# 103107, BioLegend), APC/Fire 750 anti-mouse CD3 (clone 17A2, 1:100, Cat# 100247, BioLegend), Brilliant Violet 421 anti-mouse CD4 (clone GK1.5, 1:100, Cat# 100437, BioLegend), Alexa Fluor 700 anti-mouse CD19 (clone 6D5, 1:100, Cat# 115527, BioLegend), APC anti-mouse Siglec-F (clone S17007L, 1:100, Cat# 155507, BioLegend), PE/Cyanine7 anti-mouse/human CD11b (clone M1/70, 1:100, Cat# 101215, BioLegend), and Brilliant Violet 650 anti-mouse Ly-6G (clone 1A8, 1:100, Cat# 127641, BioLegend). Data were acquired on a CytoFLEX LX flow cytometer (Beckman Coulter). All flow cytometry data were analyzed using FlowJo software (Tree Star).

Statistical analysis

Statistical analyses were performed using Prism version 9 (GraphPad Software). Data are presented as mean and 95% confidence interval. Ordinary one-way ANOVA was used for comparisons among multiple groups. Two-sided Student's t-tests were

Corrected Proof

used for comparisons between two groups. For time-course flow cytometry analyses involving multiple time point comparisons, two-sided Student's t-tests with false discovery rate (FDR) correction were applied at each time point. A P value < 0.05 was considered statistically significant.

References

1. Xu H, Guo L, Hao T, et al. Nasal solitary chemosensory cells govern daily rhythm in mouse model of allergic rhinitis. J Allergy Clini Immunol. 2024;154(3):707-18.
2. Ryu J, Yoo J, Kim M, et al. Distinct TLR-mediated pathways regulate house dust mite-induced allergic disease in the upper and lower airways. J Allergy Clini Immunol. 2013;131(2):549-61.
3. Ito K, Kanemitsu Y, Ueda T, et al. Comorbid functional dyspepsia reflects IL-33-mediated airway neuronal dysfunction in asthma. J Allergy Clini Immunol. 2024;154(6):1422-33.
4. Binshtok AM, Bean BP, Woolf CJ. Inhibition of nociceptors by TRPV1-mediated entry of impermeant sodium channel blockers. Nature. 2007;449(7162):607-10.
5. Jiang H, Cui H, Chen M, et al. Divergent sensory pathways of sneezing and coughing. Cell. 2024;187(21):5981-97.
6. Kim HY, Kim K, Li HY, et al. Selectively targeting pain in the trigeminal system. Pain. 2010;150(1):29-40.
7. Li F, Jiang H, Shen X, et al. Sneezing reflex is mediated by a peptidergic pathway from nose to brainstem. Cell. 2021;184(14):3762-73.
8. Almanzar N, Yang D, Xia J, et al. Vagal TRPV1(+) sensory neurons protect against influenza virus infection by regulating lung myeloid cell dynamics. Science Immunol. 2025;10(110):eads6243.
9. Lin J, Chen D, Guan L, et al. House dust mite exposure enhances immune responses to ovalbumin-induced intestinal allergy. Sci Rep. 2022;12(1):5216.

Corrected Proof

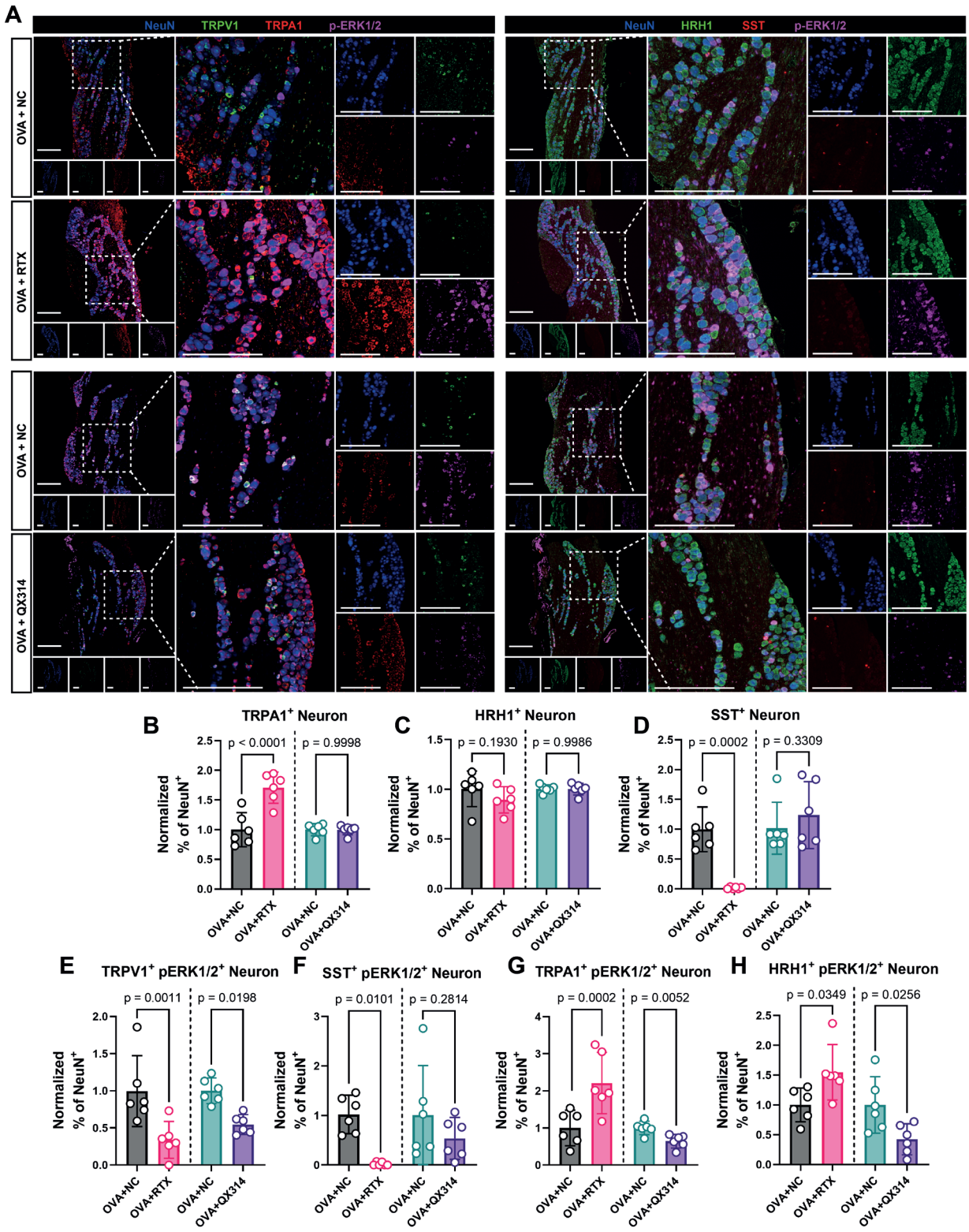

Figure S1. Divergent effects of RTX and QX-314 on trigeminal ganglion neuronal subpopulations and activation. (A) Representative immunofluorescence staining for TRPV1, TRPA1, SST, HRH1, and p-ERK1/2 in trigeminal ganglion sections following RTX or QX-314 treatment. Scale bar = 250 μm. (B–D) Quantification of the proportion of TRPA1$^+$, HRH1$^+$, and SST$^+$ neurons in trigeminal ganglia from control, RTX-treated, and QX-314-treated mice. (E–H) Quantification of the proportion of activated (p-ERK1/2$^+$) TRPV1$^+$, SST$^+$, TRPA1$^+$, and HRH1$^+$ subpopulations. Data are presented as mean and 95% confidence interval. Ordinary one-way ANOVA was used for comparisons among multiple groups. Abbreviations: TRPA1, transient receptor potential ankyrin 1; SST, somatostatin; HRH1, histamine receptor H1; p-ERK1/2, phosphorylated extracellular signal-regulated kinase 1/2; RTX, resiniferatoxin.

Corrected Proof

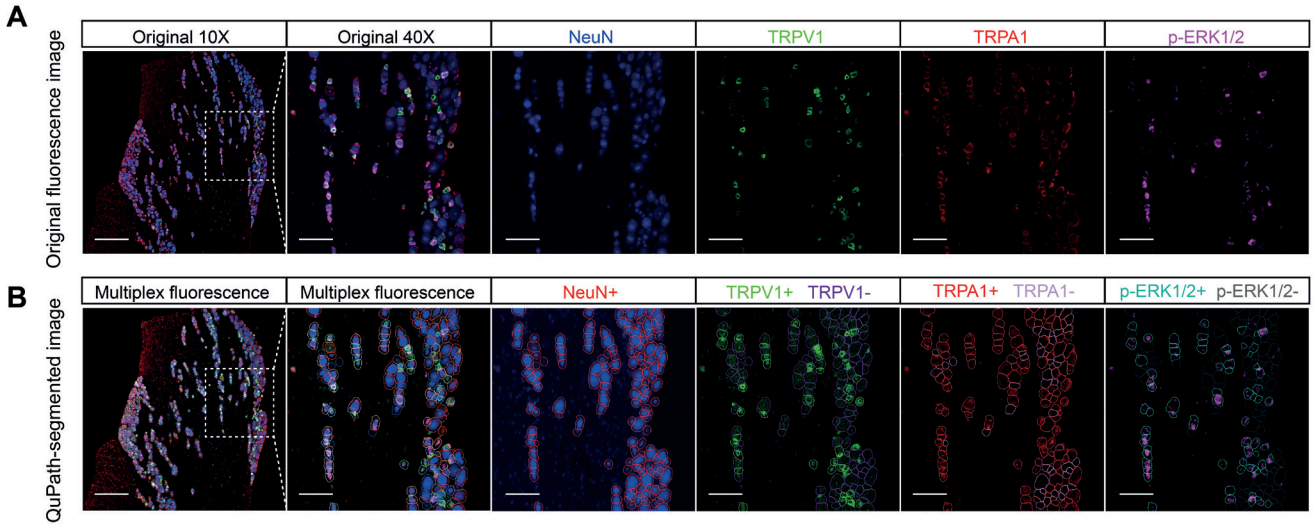

Figure S2. Multiplex immunofluorescence analysis of trigeminal ganglion neurons. (A) Representative original fluorescence images at 10× and 40× magnification showing NeuN, TRPV1, TRPA1, and p-ERK1/2 staining in trigeminal ganglion sections. (B) Representative images illustrating the segmentation and classification workflow using QuPath software. Neuronal somata were segmented and detected based on NeuN-positive regions. Individual fluorescence channels were then classified as positive or negative under consistent threshold settings. The classification results from all channels were merged to determine the combination of markers expressed by each neuronal soma. Scale bars: 250 μm for 10× images; 62.5 μm for 40× images. Abbreviations: NeuN, neuronal nuclei; p-ERK1/2, phosphorylated extracellular signal-regulated kinase 1/2; TRPA1, transient receptor potential ankyrin 1; TRPV1, transient receptor potential vanilloid 1.